

Current-driven ferromagnetic resonance, mechanical torques and rotary motion in magnetic nanostructures

Alexey A. Kovalev,¹ Gerrit E. W. Bauer,¹ and Arne Brataas^{2,3}

¹*Kavli Institute of NanoScience, Delft University
of Technology, 2628 CJ Delft, The Netherlands*

²*Department of Physics, Norwegian University of
Science and Technology, NO-7491 Trondheim, Norway*

³*Center for Advanced Study at the Norwegian Academy of Science and Letters,
Drammensveien 78, NO-0271 Oslo, Norway*

(Dated: October 30, 2018)

Abstract

We study theoretically the detection and possible utilization of electric current-induced mechanical torques in ferromagnetic-normal metal heterostructures generated by spin-flip scattering or the absorption of transverse spin currents by a ferromagnet. To this end, we analyze the DC voltage signals over a spin valve driven by an AC current. In agreement with recent studies, this “rectification”, measured as a function of AC frequency and applied magnetic field, contains important information on the magnetostatics and -dynamics. Subsequently, we show that the vibrations excited by spin-transfer to the lattice can be detected as a splitting of the DC voltage resonance. Finally, we propose a concept for a spin-transfer-driven electric nanomotor based on integrating metallic nanowires with carbon nanotubes, in which the current-induced torques generate a rotary motion

PACS numbers: 76.50.+g, 72.25.Ba, 85.85.+j

I. INTRODUCTION

An electromotor is an apparatus that generates rotational motion with electrical currents, as demonstrated by Faraday in 1821. Under miniaturization, the torques generated by Ørsted magnetic fields scale unfavorably compared to the increased friction, rendering the Faraday motor an unfeasible concept at the nanoscale. Alternative concept for nanomachines are based on electrostatic forces,¹ thermal fluctuations,² torques induced by circularly polarized light³ and angular momentum transfer by spin-polarized currents.^{4–7} In this article, we elaborate on the last idea.

A spin-polarized current carries an angular momentum current:

$$T_{SP} = PI\hbar/(2e) = PT_0 \quad (1)$$

where $P = (I_{\uparrow} - I_{\downarrow})/I$ is the polarization of the charge current $I = I_{\uparrow} + I_{\downarrow}$, e is the electron charge and $T_0 = I\hbar/(2e)$. If transferred completely to the lattice, mechanical torques are created of the same magnitude, which can be relatively large in nanoscale structures. Since spin currents are routinely excited in magnetoelectronic devices such as spin valves, we pose here the question whether current-induced mechanical torques can be detected and utilized in such structures. We conclude that the resonant magnetomechanical coupling studied earlier^{6,8} should indeed be observable in spin valve structures, paving the way for applications such as high frequency actuators and transducers of mechanical motion. Furthermore, we propose a design for a spin-transfer driven electric nanomotor based on carbon nanotubes.³

The resonant rectification of a current in spin valve as a function of an applied AC frequency has been found experimentally to form a rich source of information about the magnetization dynamics in spin valve structures.^{9,10} Kupferschmidt *et al.* found theoretically that the spin-pumping by the magnetization dynamics¹¹ significantly modify these spectra.³⁵ We suggest that the AC-DC conversion in spin valves can be used to detect vibrational modes excited by the spin-polarized currents.

In this manuscript, we address the theory of spin valves excited by AC currents, show how to include the effects of the magnetovibrational coupling, and predict signatures of the current-induced mechanical torques. We also share our ideas how these torques could drive a rotary (rather than vibrational) motion, *i.e.* an electric nanomotor. The manuscript is organized as follows. In Sec. II, we calculate (position-dependent) mechanical torques generated

by the spin-flip dissipation of a spin current injected by a ferromagnet into a normal metal. In Sec. III, we study the spin-transfer mechanical torques resulting from the absorption of transverse spin-currents by a ferromagnet. We suggest to employ the recently reported diode effect^{9,10} in F(erro)magnet)|N(ormal)|F(erro)magnet) metal spin valves to detect the vibrations created by spin-transfer mechanical torques. We calculate the nonlinear DC voltage emanating from the spin-transfer driven ferromagnetic resonance with and without the resonant magnetovibrational coupling. Spin transfer torques non-collinear with planes formed by principal axis of anisotropies can deform the resonant line shape of DC voltage as a function of the AC current bias frequency. In Appendix B and C, we calculate the extra DC voltage caused by spin-pumping and prove that it can play a key role in sufficiently thin films. In Appendix B, we also conclude that the magnetovibrational coupling is observable by virtue of the spin-pumping even in asymmetric N|F|N heterostructures. In Sec. IV, we propose a spin-transfer driven nanomotor concept based on integrating metallic nanowires with carbon nanotubes.

II. MECHANICAL TORQUES DUE TO DISSIPATION OF SPIN CURRENTS

Consider a normal-metal diffusive wire or nanostructured pillar into which a spin accumulation has been injected via an electrically biased ferromagnetic contact (Fig. 1). Spin \mathbf{I}_s and charge I_0 currents can be conveniently related via 2×2 -matrices in Pauli spin space $\hat{I} = (\hat{1}I_0 + \hat{\sigma} \cdot \mathbf{I}_s)/2$, where $\hat{\sigma}$ is the vector of Pauli spin matrices and $\hat{1}$ is the 2×2 unit matrix. Spin-orbit interactions or magnetic impurities cause spin-flip scattering that can be parametrized by a spin-flip relaxation time t_{sf} . $\boldsymbol{\mu}_s$, the local (vector) spin accumulation is related to the spin current density $\mathbf{j}_s = \mathbf{I}_s/(eS)$ (e is the electron charge and S is the cross-section of the wire) by the angular momentum conservation law:

$$\frac{\partial}{\partial t} \boldsymbol{\mu}_s + \frac{\partial}{\partial y} \frac{\mathbf{j}_s}{\mathcal{N}} = \frac{\boldsymbol{\mu}_s}{t_{sf}}. \quad (2)$$

The dissipated angular momentum per unit length, $\boldsymbol{\tau} = (\hbar/2) S \mathcal{N} \boldsymbol{\mu}_s / t_{sf}$, where \mathcal{N} is the density of states at the Fermi-level, is transferred as a mechanical torque to the lattice. In the configuration sketched in Fig. 1, the injected spin accumulation $|\mu_s| = \mu_s$ and the mechanical torque are polarized in the y -direction. Newton's Law for the mechanical motion

of the substrate then reads¹²

$$\rho I \frac{\partial^2 \varphi(y, t)}{\partial t^2} = C \frac{\partial^2 \varphi(y, t)}{\partial y^2} + \frac{\hbar}{2} S \mathcal{N} \frac{\mu_s(y, t)}{t_{sf}} \quad (3)$$

where $\varphi(y, t)$ is the angle of torsion, $I = I_x + I_z$ ($I_z = \int x^2 dz dx$, $I_x = \int z^2 dz dx$) is the moment of inertia of the cross-section at y relative to its center of mass, ρ is the mass density, C is an elastic constant defined by the shape and material of the wire ($C = \mu R^4/2$ for a circular cross section with radius R , μ is the Lamé constant). Eq. (3) must be complemented by the boundary conditions ($\varphi = 0$) at the clamping points.

We now concentrate on a bimetal wire consisting of a ferromagnetic and a normal metal (Fig. 1). We assume for simplicity here that the bulk resistances of the wires are much larger than the interface resistance (Ref. 14 shows how interfaces can be taken into account) to the extent that we may disregard the latter. The magnetization and mechanical motion is much slower than the relaxation scattering, therefore, we can consider only the parametrically stationary limit. The charge current density j_0 is conserved ($\partial_y j_0 = 0$) and Eq. (2) reduces to

$$\frac{\partial}{\partial y} \mathbf{j}_s = \frac{\mathcal{N} \boldsymbol{\mu}_s}{t_{sf}} = \frac{2\boldsymbol{\tau}}{\hbar S}. \quad (4)$$

In the normal metal, charge and spin currents are governed by Fick's Laws $j^N = \mathcal{N}^N D^N \partial_y \mu_0^N$ and $\mathbf{j}_s^N = \mathcal{N}^N D^N \partial_y \boldsymbol{\mu}_s^N$ respectively, where D^N is the diffusion constant and the index N indicates the normal metal, leading to the diffusion equations:

$$\frac{\partial^2}{\partial y^2} \mathcal{N}^N D^N \mu_0^N = 0, \quad \frac{\partial^2}{\partial y^2} \mathcal{N}^N D^N \boldsymbol{\mu}_s^N = \mathcal{N}^N \boldsymbol{\mu}_s^N / t_{sf}^N = \frac{\boldsymbol{\tau}_N}{\frac{\hbar}{2} S}.$$

where τ_N is the mechanical torque per unit length for the normal metal. In a ferromagnet (F), the particle and spin currents are $j^F = (\mathcal{N}_\uparrow^F D_\uparrow^F \partial_y \mu_\uparrow + \mathcal{N}_\downarrow^F D_\downarrow^F \partial_y \mu_\downarrow)/2$ and $\mathbf{j}_s^F = \mathbf{m} \partial_y (\mathcal{N}_\uparrow^F D_\uparrow^F \mu_\uparrow - \mathcal{N}_\downarrow^F D_\downarrow^F \mu_\downarrow)/2$, where $D_{\uparrow(\downarrow)}^F$ is the diffusion constants for spin-up (-down) electrons and $\mathcal{N}_{\uparrow(\downarrow)}^F$ is the corresponding spin-up (-down) density of states. The diffusion equation in a ferromagnet then reads:

$$\frac{\partial^2}{\partial y^2} (\mathcal{N}_\uparrow^F D_\uparrow^F \mu_\uparrow + \mathcal{N}_\downarrow^F D_\downarrow^F \mu_\downarrow) = 0, \quad \frac{\partial^2}{\partial y^2} (\mathcal{N}_\uparrow^F D_\uparrow^F \mu_\uparrow - \mathcal{N}_\downarrow^F D_\downarrow^F \mu_\downarrow) = \mathcal{N}^F (\mu_\uparrow - \mu_\downarrow) / t_{sf}^F,$$

leading to

$$\frac{\partial^2}{\partial y^2} D^F (\mu_\uparrow - \mu_\downarrow) = (\mu_\uparrow - \mu_\downarrow) / t_{sf}^F = \tau_F / \left[\frac{\hbar}{2} S \mathcal{N}^F \right],$$

where τ_F is the mechanical torques per unit length for the ferromagnetic metal, $D^F = 2D_\uparrow^F D_\downarrow^F \mathcal{N}_F / (\mathcal{N}_\uparrow^F D_\uparrow^F + \mathcal{N}_\downarrow^F D_\downarrow^F)$ and $\mathcal{N}^F = (\mathcal{N}_\uparrow^F + \mathcal{N}_\downarrow^F)/2$.

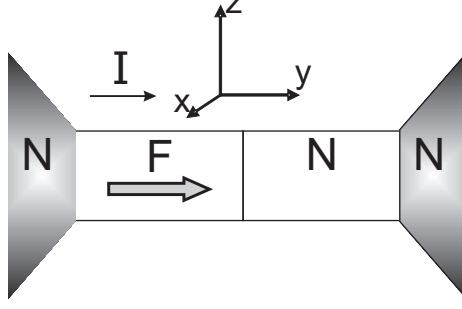


Figure 1: Spin transfer from spin-polarized currents to the lattice in a heterostructure consisting of two (ferromagnetic and normal metal) sections connected to mechanically clamped normal and ferromagnetic metal reservoirs. Polarized currents lead to torques twisting the middle section.

We can now calculate the mechanical torques by solving the diffusion equations, requiring the continuity of distribution functions and conservation of the spin and charge currents at the interface.^{13,14} We also require no spin accumulation at the connection with reservoirs. For the ferromagnetic ($y < 0$) and normal ($y > 0$) metals we find, respectively:

$$\tau_F(y) = T_0 \frac{P \sinh[(L_F + y)/l_{sd}^F] / \sinh(L_F/l_{sd}^F)}{l_{sd}^F \coth(L_F/l_{sd}^F) + v l_{sd}^N \coth(L_N/l_{sd}^N)}, \quad (5)$$

$$\tau_N(y) = T_0 \frac{v P \sinh[(L_N - y)/l_{sd}^N] / \sinh(L_N/l_{sd}^N)}{l_{sd}^F \coth(L_F/l_{sd}^F) + v l_{sd}^N \coth(L_N/l_{sd}^N)}, \quad (6)$$

where $P = (G_{\uparrow} - G_{\downarrow}) / (G_{\uparrow} + G_{\downarrow})$ is the current polarization of the ferromagnet here defined in terms of the spin-up and spin-down conductances G_{\uparrow} and G_{\downarrow} , $l_{sd}^F = \sqrt{D^F t_{sf}^F}$ and $l_{sd}^N = \sqrt{D^N t_{sf}^N}$ are the spin-diffusion lengths in the ferromagnet and normal metals, respectively, and T_0 has been introduced in Eq. (1), L_F and L_N are the lengths of the ferromagnet and normal metals respectively, and $v = [\mathcal{N}_N t_{sf}^N] / [\mathcal{N}_F t_{sf}^F]$. For the configuration sketched in Fig. 1, the mechanical torque is directed along the y axis. The torque density is discontinuous when $v \neq 1$. As shown in Fig. 2, the mechanical torques are enhanced close to the F|N interface on the scale defined by the spin-diffusion length in both ferromagnet and normal metals. The mechanical torques change sign with the electric currents direction.

Integrating Eqs. (5,6) leads to the total torque acting on the wire:

$$T_F = T_0 \frac{P l_{sd}^F \tanh(L_F/2l_{sd}^F)}{l_{sd}^F \coth(L_F/l_{sd}^F) + v l_{sd}^N \coth(L_N/l_{sd}^N)}, \quad (7)$$

$$T_N = T_0 \frac{v P l_{sd}^N \tanh(L_N/2l_{sd}^N)}{l_{sd}^F \coth(L_F/l_{sd}^F) + v l_{sd}^N \coth(L_N/l_{sd}^N)}. \quad (8)$$

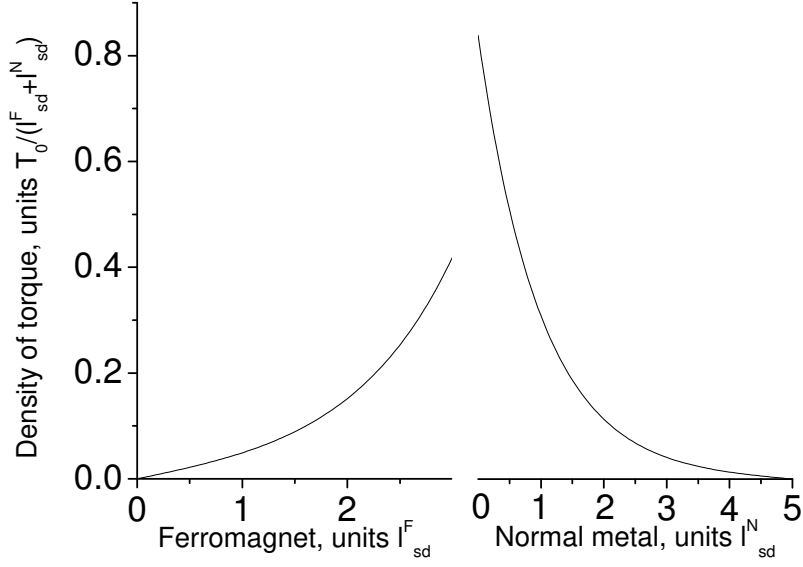


Figure 2: The mechanical torque per unit length along the F|N wire; $P = 0.7$, $l_{sd}^F = 10\text{nm}$, $l_{sd}^N = 20\text{nm}$, $L_F/l_{sd}^F = 3$, $L_N/l_{sd}^N = 5$, and $v = 2$.

When $L_F \gg l_{sd}^F$ and $L_N \gg l_{sd}^N$, we obtain $T_{SP} = T_F + T_N = P\tau_0$ as expected by the complete dissipation of the spin current in this limit (Eq. (1)). By ultrasensitive displacement detection, it should be possible to observe the mechanical strain caused by the spin-flip torques⁴ in the setup of Fig. 1.

III. GENERATION AND DETECTION OF THE MECHANICAL TORQUES DUE TO SPIN TRANSFER

In the previous section, we studied mechanical torques arising from spin-flip relaxation processes within the bulk of the metals. In contrast, in this section, we will consider structures (see Fig. 3) in which the spin transfer is dominated by dephasing processes (leading to absorption of transversely polarized currents)¹³ at the normal metal|ferromagnetic interfaces, whereas the spin-flip processes in the bulk materials are disregarded (which can be repaired easily if necessary). Such a device is superior to the wires of the previous section in generating mechanical torques when the structures are smaller than the spin-diffusion length. We propose here to induce and detect the magneto-vibrational modes⁸ driven by spin-transfer torques in devices such as shown in Fig. 3, *i.e.* a doubly clamped heterostructure in the

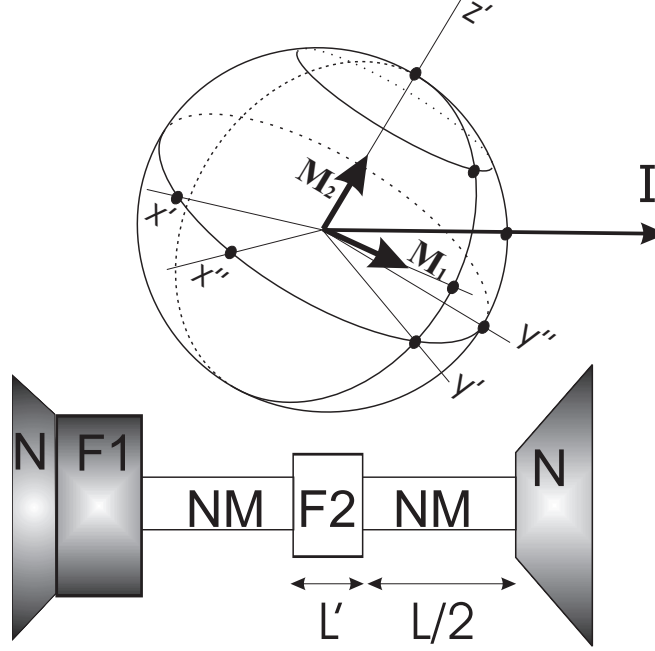


Figure 3: Model sample to study spin transfer to the lattice consisting of ferromagnets (F1 and F2) and NM, *i.e.* tunnel junctions or normal metal). F1 and the normal metal N are electron reservoirs that are mechanically clamped. The vector diagram shows the reference frames used in calculations with respect to the magnetizations. The magnetization of F1 is fixed, $\mathbf{M}_1 \equiv \mathbf{M}_{\text{fixed}}$, and that of F2 is variable, $\mathbf{M}_2 \equiv \mathbf{M}$.

shape of a bar with a ferromagnetic load in the center. In our set-up, the mechanical torque is generated in the ferromagnet F2 by the transversely polarized spin current (ferromagnet F1 is supposed to be clamped by the substrate). The absorbed spin-angular momentum is transferred to the lattice by the magnetic shape and crystal anisotropies. In the regime of the resonant magnetovibrational coupling, the mechanical motion is strongly affected by the magnetization dynamics created by spin-transfer torques,⁸ which, in turn affect the transport properties. We predict that such vibrations should be detectable by current-driven ferromagnetic resonance experiments reported in Refs. 9 and 10. We start by analyzing the DC voltage signals over a spin valve resulting from the “rectification” of an AC current by the precessing magnetization (without magnetovibrational coupling, *e.g.* setups from Refs. 9 and 10) as an intermediate step. A general analysis of the DC signals in the regime of the resonant magnetovibrational coupling is subsequently given. We also estimate the maximum torques that can be created in these structures.

The derivation below is carried out for a system in which the ferromagnet F2 is inserted into the normal metal island. However, the rectification of the AC current and the excitation of magnetovibrational modes also occur (and can be treated by our methods) in a system in which the ferromagnet is attached to the side or on top of the normal metal wire (“spin-flip transistor”).^{15,16}

A. Ferromagnetic resonance driven by spin-transfer torques

Initially, we assume that the mechanical modes are not excited in the device depicted in Fig. 3. One (the “hard”) layer magnetization of F1 is assumed completely fixed by shape or crystal anisotropies to the direction $\mathbf{M}_1 = \mathbf{M}_{\text{fixed}}$ with unit vector $\mathbf{m}_{\text{fixed}}$. We are interested in the dynamics of the magnetization direction $\mathbf{m} = \mathbf{M}_2/M_s$ of the middle (“soft”) layer F2, where $|\mathbf{M}_2| = M_s$ is the constant saturation magnetization, in the presence of an AC electric current bias. We consider the soft layer to be at resonance,¹⁰ but note that the soft and hard layers can exchange their roles as a function of frequency (*e.g.* in Fig. 5). We model the magnetization dynamics by the generalized Landau-Lifshitz-Gilbert (LLG) equation in the macrospin approximation that is augmented by the current-dependent spin-transfer torque:¹⁷

$$\frac{d\mathbf{M}}{dt} = -\gamma \mathbf{M} \times \mathbf{H}_{\text{eff}} + \frac{\alpha}{M_s} \mathbf{M} \times \left(\frac{d\mathbf{M}}{dt} \right) + \gamma \frac{\hbar}{2e} \frac{I(t)}{V_m} [\eta_1 \mathbf{m} \times (\mathbf{m}_{\text{fixed}} \times \mathbf{m}) + \eta_2 (\mathbf{m}_{\text{fixed}} \times \mathbf{m})], \quad (9)$$

where $I(t)$ is the time dependent current through the system, η_1 describes the efficiency of conventional spin transfer, and η_2 parametrizes an “effective spin-transfer exchange field”. When the spacer is an insulator, as in the experiment of the Tsukuba group,⁹ the parameter η_1 is a constant governed by the expressions such as derived by Slonczewski.¹⁸ The “effective field” η_2 has been less well investigated in magnetic tunnel junctions and is treated here as an adjustable parameter. When the spacer is a normal metal in a configuration sketched in Fig. 3, the LLG equation for the soft layer reads:

$$\frac{d\mathbf{M}}{dt} = -\gamma \mathbf{M} \times \mathbf{H}_{\text{eff}} + \frac{\alpha}{M_s} \mathbf{M} \times \left(\frac{d\mathbf{M}}{dt} \right) - \frac{\gamma \hbar}{2eV_m} \mathbf{m} \times [(\mathbf{I}_{s1} + \mathbf{I}_{s2}) \times \mathbf{m}] \quad (10)$$

where the spin currents leaving the soft ferromagnet can be computed by magnetoelectronic circuit theory¹³ as

$$I_{1(2)} = (G_{\uparrow} + G_{\downarrow})(\mu_0^{2(1)} - \mu_0^{1(2)}) + (G_{\uparrow} - G_{\downarrow})(\boldsymbol{\mu}_s^{2(1)} - \boldsymbol{\mu}_s^{1(2)}) \cdot \mathbf{m} \quad (11)$$

$$\begin{aligned} \mathbf{I}_{s1(2)} = \mathbf{m} & \left[(G_{\uparrow} - G_{\downarrow})(\mu_0^{2(1)} - \mu_0^{1(2)}) + (G_{\uparrow} + G_{\downarrow})(\boldsymbol{\mu}_s^{2(1)} - \boldsymbol{\mu}_s^{1(2)}) \right] \\ & - (2\mathbf{m} \times \boldsymbol{\mu}_s^{1(2)}) \times \mathbf{m} G_r - (2\mathbf{m} \times \boldsymbol{\mu}_s^{1(2)}) G_i, \end{aligned} \quad (12)$$

where α is the Gilbert damping constant, γ is the gyromagnetic ratio, G_{\uparrow} and G_{\downarrow} describe the conventional spin-dependent conductances limited by bulk and interface scattering and $G_{\uparrow\downarrow} = G_r + iG_i$ is the interface mixing conductance of the ferromagnet, μ_0 and $\boldsymbol{\mu}_s$ are the chemical potential and spin-accumulation in the normal metals, respectively, the spin $\mathbf{I}_{s1(2)}$ and charge $I_{1(2)}$ currents correspond to the current (spin) flow into the normal metal node 1(2). It is shown in Appendix A that Eqs. (9) and (10) are equivalent when we allow for an angle dependence of the parameters $\eta_{1(2)}$. The efficiencies of the spin-transfer torque $\eta_1(\theta)^{14}$ and the “effective spin-transfer field” $\eta_2(\theta)$ mainly depend on the real and imaginary part of the mixing conductance, respectively.

Choosing the z' -axis along the equilibrium direction (\mathbf{M}_0) of the soft layer and the x' -axis perpendicular to both magnetizations (see Fig. 3), we expand the free energy close to the equilibrium direction of the magnetization as

$$F(\mathbf{M}) = F(\mathbf{M}_0) + N_{x'} M_{x'}^2/2 + N_{y'} M_{y'}^2/2 + N_{x'y'} M_{x'} M_{y'} \quad (13)$$

such that the effective magnetic field

$$\mathbf{H}_{\text{eff}} = -\partial F/\partial \mathbf{M} = -(N_{x'} M_{x'} + N_{x'y'} M_{y'}) \mathbf{x}' - (N_{y'} M_{y'} + N_{x'y'} M_{x'}) \mathbf{y}' \quad (14)$$

where $N_{x'}$, $N_{y'}$, and $N_{x'y'}$ are parameters characterizing the energy of the macrospin excitations. The free energy Eq. (13) is not diagonal in the basis of the magnetizations along the x' and y' axis, but can be diagonalized in another basis rotated by the angle ϕ around the z' -axis, so that $N_{x'} = N_x^d \cos^2 \phi + N_y^d \sin^2 \phi$, $N_{y'} = N_y^d \cos^2 \phi + N_x^d \sin^2 \phi$, $N_{x'y'} = (N_x^d - N_y^d) \cos \phi \sin \phi$. Here, N_x^d and N_y^d are the eigenvalues of the expansion tensor in Eq. (13). We consider here an arbitrary direction of an external magnetic field \mathbf{H}_0 . In general, the components of \mathbf{H}_0 contribute to Eq. (13) in a non-trivial way. As an illustration let us consider an external field along the z -axis, which can be included as follows: $N_{x'} = N_{x'}^0 + H_0/M_s$ and $N_{y'} = N_{y'}^0 + H_0/M_s$, where $N_{x(y)}^0$ are elements of the magnetic anisotropy tensor.

The linear response of the magnetization to an AC current perturbation is given by the

response functions $\chi_{x'I} = (M_{x'}/I)_\omega$ and $\chi_{y'I} = (M_{y'}/I)_\omega$. From Eqs. (9,14)

$$\chi_{x'I}(\omega) = \frac{\hbar\gamma \sin \theta}{2eV_m} \frac{i\eta_2\omega + \gamma M_s \Gamma_{x'}}{\omega^2(1 + \alpha^2) - \omega_m^2 + 2i\alpha'\omega\omega_m}, \quad (15)$$

$$\chi_{y'I}(\omega) = \frac{\hbar\gamma \sin \theta}{2eV_m} \frac{-i\eta_1\omega + \gamma M_s \Gamma_{y'}}{\omega^2(1 + \alpha^2) - \omega_m^2 + 2i\alpha'\omega\omega_m}, \quad (16)$$

where V_m is the volume of the magnet, $\omega_m^2 = \gamma^2 N_x^d N_y^d M_s^2 = \gamma^2 M_s^2 (N_{x'} N_{y'} - N_{x'y'}^2)$, $\Gamma_{x'} = \eta_1(N_{y'} + N_{x'y'}\alpha) + \eta_2(N_{x'y'} - N_{y'}\alpha)$, $\Gamma_{y'} = \eta_1(N_{x'y'} + N_{x'}\alpha) + \eta_2(N_{x'} - N_{x'y'}\alpha)$, and the damping parameter is modified by the anisotropies as

$$\alpha' = \alpha \frac{(N_x^d + N_y^d)/2}{\sqrt{N_x^d N_y^d}} = \alpha \frac{(N_{x'} + N_{y'})/2}{\sqrt{N_{x'} N_{y'} - N_{x'y'}^2}}. \quad (17)$$

From Eqs. (15,16), we conclude that both the field effect η_2 , characteristic for tunnel junctions,⁹ and non-collinear anisotropies $N_{x'y'}$ cause a phase shift in the magnetization response $\chi_{y'I}(\omega)$ that is relevant to the rectification effect, as demonstrated below. At resonance, the parameters $\Gamma_{x'}$ and $\Gamma_{y'}$ are the components of the out-of-phase magnetization response.

The resulting magnetization dynamics causes oscillations of the magnetoresistance $R(\mathbf{m}_1(t), \mathbf{m}_2(t)) = R(\cos \theta(t))$ of the multilayer structure (details of the calculations are given in Appendix A). In the presence of an AC current bias $I(t) = I_0 \text{Re} e^{i\omega t}$, the resistance has an oscillating component that in the linear approximation reads:

$$R(\cos \theta(t)) \approx R(\nu) - \sin \theta \frac{\partial R(\nu)}{\partial \nu} \Delta \theta(t) \quad (18)$$

$$= R(\nu) - \sin \theta \frac{\partial R(\nu)}{\partial \nu} m_{y'}(t) = R(\nu) - \frac{I_0}{M_s} \sin \theta \frac{\partial R(\nu)}{\partial \nu} \text{Re}(e^{i\omega t} \chi_{y'I}), \quad (19)$$

leading to a nonlinear phase-sensitive effect in the voltage across the sample

$$U = R(t)I(t) = R(\nu)I(t) - \frac{\sin \theta}{4M_s} \frac{\partial R(\nu)}{\partial \nu} (I_0 e^{i\omega t} \chi_{y'I} + I_0 e^{-i\omega t} \chi_{y'I}^*) (I_0 e^{i\omega t} + I_0 e^{-i\omega t}) \quad (20)$$

$$\sim I_0^2 \text{Re}[(1 + e^{i2\omega t}) \chi_{y'I}], \quad (21)$$

where the parameter $\nu = \cos \theta$ describes the equilibrium configuration of the magnetizations and $\theta(t) = \theta + \Delta \theta(t)$ (to lowest order $\Delta \theta \approx m_{y'}$). The magnetization dynamics is thus manifest in the nonlinear response, *i.e.* the zero and second harmonic components of the voltage across the sample:

$$U_0 = \frac{I_0^2 \sin \theta}{2M_s} \frac{\partial R(\nu)}{\partial \nu} \text{Re} \chi_{y'I}(\omega) \stackrel{\omega \rightarrow \omega_m}{=} -I_0^2 \sin^2 \theta \frac{\partial R(\nu)}{\partial \nu} \frac{\hbar}{2e} \frac{\gamma}{2M_s V_m} \frac{1}{\omega_m} \times \left(\frac{\alpha' \omega_m^2}{(\omega - \omega_m)^2 + \alpha'^2 \omega_m^2} - \frac{(\omega - \omega_m) \gamma M_s \Gamma_{y'}}{(\omega - \omega_m)^2 + \alpha'^2 \omega_m^2} \right), \quad (22)$$

$$\begin{aligned}
U_{2\omega} = & \frac{I_0^2 \sin \theta}{2M_s} \frac{\partial R(\nu)}{\partial \nu} |\chi_{y'I}(\omega)| \stackrel{\omega \rightarrow \omega_m}{=} I_0^2 \sin^2 \theta \frac{\partial R(\nu)}{\partial \nu} \frac{\hbar}{2e} \frac{\gamma}{2V_m} \\
& \times \sqrt{\frac{1 + \gamma^2 M_s^2 \Gamma_{y'}/\omega^2}{(\omega - \omega_m)^2 + \alpha'^2}}.
\end{aligned} \tag{23}$$

As pointed out in Ref. 9, the DC voltage U_0 can be interpreted as a diode-like rectification. The amplitudes U_0 and $U_{2\omega}$ show a resonant enhancement close to ω_m (note that U_0 corresponds to V_{mix} in Ref. 10 and its sign corresponds to a current flow from soft to hard ferromagnetic layer). Eq. (22) is a linear combination of the symmetric and antisymmetric Lorentzians (see Fig. 4). By fitting the DC voltage $U_0(\omega)$ to a linear combination of the two curves in Fig. 4, we can determine the parameter $\Gamma_{y'} \approx \eta_1 N_{x'y'} + \eta_2 N_{x'}$ that is affected by the effective field η_2 and the non-collinear anisotropy $N_{x'y'}$. In Fig. 5, we demonstrate how the resonance becomes skewed merely by the non-collinear shape anisotropy (the spin-transfer torque does not lie in a plane formed by principal axes of the shape anisotropy). The resonant layer with the magnetization \mathbf{M}_2 corresponds to the harder layer in this plot (as it was discussed in Sec. IIIA, the harder and softer layers can switch their roles with a proper choice of the AC current frequency). The opposite scenario,⁹ without anisotropies, the effective field η_2 can still cause an antisymmetric Lorentzian signal since $\Gamma_{y'} \approx \eta_2 N_{x'} = \eta_2 H_0/M_s$, as reported by Ref. 35.

B. Magnetovibrational resonance driven and detected by spin-transfer torques

In the following, we repeat the derivation of the previous section but allow for a torsional degree of freedom along the current flow. This requires a free-standing conducting structure, such as a doubly clamped cantilever. We already discussed the coupled dynamics of the magnetization and the lattice for a small magnet at the free tip of a cantilever that is clamped on the other side.⁸ However, here we consider the limit in which the magnet is heavy compared to the cantilever. This reduces the mechanical resonance frequencies, but increases the magnetomechanical coupling strength. The normal metal lattice serves as a spring and the ferromagnet is the load. We first consider a well-aligned structure for which the primed and unprimed coordinate systems in Fig. 6 coincide. A mechanical torsion

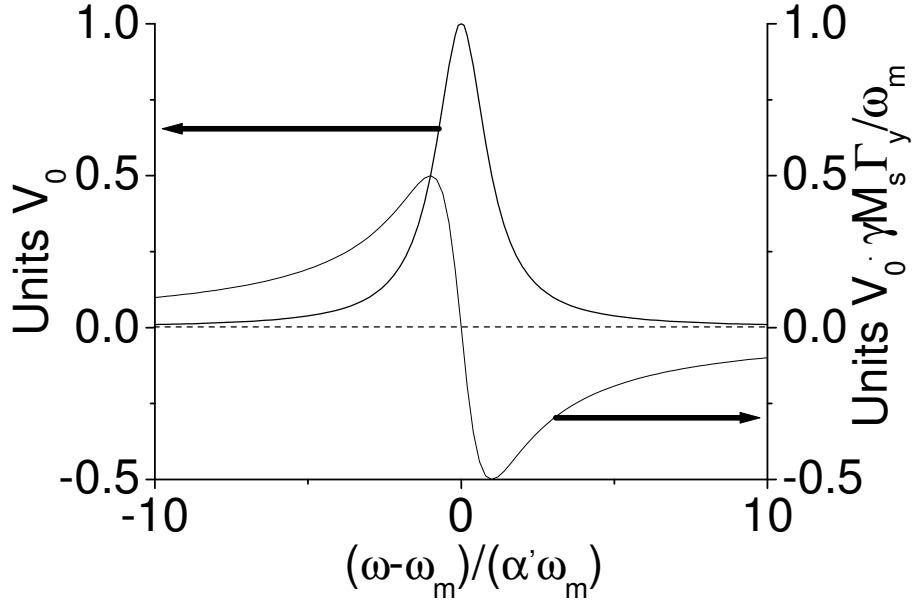


Figure 4: The dimensionless DC voltage over the sample biased by an AC current has two components that are plotted as a function of AC current frequency; $V_0 = I_0^2 \sin^2 \theta \frac{\partial R(\nu)}{\partial \nu} \frac{\hbar}{2e} \frac{\gamma}{2M_s V_m} \frac{1}{\alpha' \omega_m}$.

profile described by the angle $\varphi(y)$ increases the free energy as:

$$F(\mathbf{M}) = F(\mathbf{M}_0) + V_m (N_x [M_x + M_z \varphi(0)]^2 / 2 + N_y M_y / 2 + N_{xy} [M_x + M_z \varphi(0)] M_y) + \frac{C}{2} \int_{-L/2}^{L/2} \left(\frac{\partial \varphi}{\partial y} \right)^2 dy, \quad (24)$$

where C is an elastic constant defined by the shape of the cross-section and the material of the normal metal link ($C = \mu d a^3 / 3$ for a long plate with thickness a much smaller than width d , $a \ll d$, μ is the Lamé constant for the normal metal), $\varphi(0)$ is the torsion angle at the middle magnetic section. The coefficients N_x , N_y and N_{xy} have the same meaning as in the previous section (one expects $N_{xy} = 0$ in setup of Fig. 6; however, we keep N_{xy} in order to use our results for more general configurations). The width L' of the magnetic layer along the axis y is supposed to be small compared to the length of the normal metal links $L (\gg L')$, so internal strains and deformations in the magnetic section are disregarded. The integration is therefore carried out from one clamping point $y = -L/2$ to the other at $y = L/2$, excluding the ferromagnetic layer. With Eq. (24), the Landau-Lifshitz-Gilbert

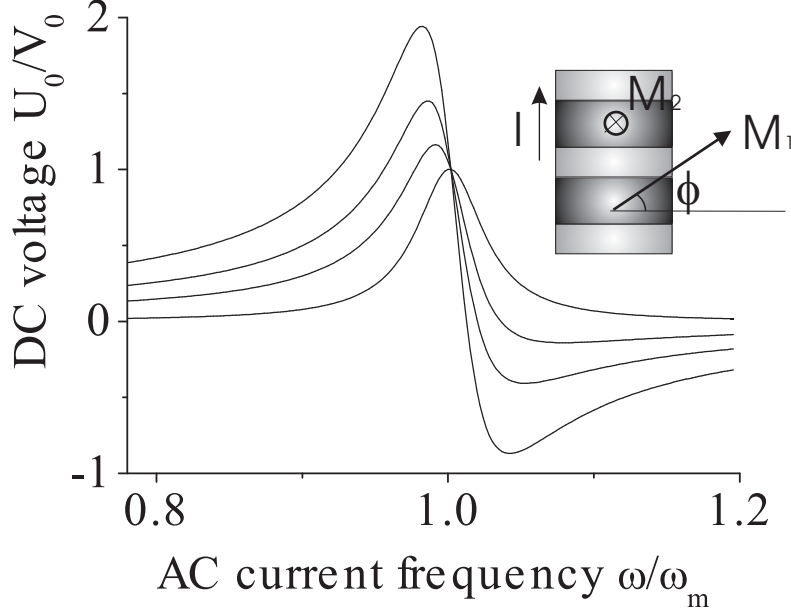


Figure 5: The resonance peaks are skewed when the spin-transfer torque does not lie in a plane formed by principal axes of the shape anisotropy. We illustrate this by exciting the magnetization \mathbf{M}_2 of the harder (resonant) layer with an easy plane anisotropy by AC currents, while the soft layer magnetization is forced into the directions $\phi = 0 : \pi/20 : \pi/10 : \pi/4$ by an external magnetic field. Here $\eta_2 = 0$.

equation has to be modified as:

$$\frac{d\mathbf{M}}{dt} = -\gamma \mathbf{M} \times \mathbf{H}_{\text{eff}} + \frac{\alpha}{M_s} \mathbf{M} \times \left(\frac{d\mathbf{M}}{dt} \right)_m + \gamma \frac{\hbar}{2e} \frac{I(t)}{V_m} [\eta_1 \mathbf{m} \times (\mathbf{m}_{\text{fixed}} \times \mathbf{m}) + \eta_2 (\mathbf{m}_{\text{fixed}} \times \mathbf{m})] \quad (25)$$

$$\mathbf{H}_{\text{eff}} = -(N_x M_x + N_{xy} M_y + N_x M_z \varphi(0)) \mathbf{x} \quad (26)$$

$$- (N_y M_y + N_{xy} M_x + N_{xy} M_z \varphi(0)) \mathbf{y}, \quad (27)$$

where the derivative $(d\mathbf{M}/dt)_m$ is defined in the reference frame of the magnet, since most proposed mechanisms for Gilbert damping act on the magnetization motion relative to the underlying lattice only. This can be taken into account by

$$\left(\frac{d\mathbf{M}}{dt} \right)_m = \frac{d\mathbf{M}}{dt} - \frac{d\varphi(0)}{dt} M_z \mathbf{x}. \quad (28)$$

The equation of mechanical torsional motion of the normal metal strip is:¹²

$$C \frac{\partial^2 \varphi}{\partial y^2} = \rho I \frac{\partial^2 \varphi}{\partial t^2}, \quad (29)$$

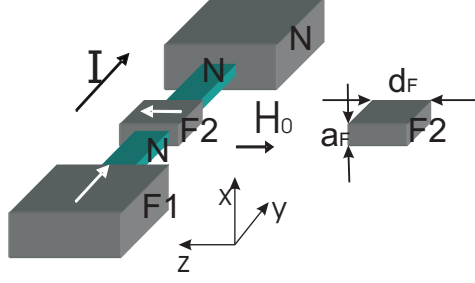


Figure 6: A device to detect magnetovibrational coupling caused by magnetic form and crystal anisotropies. An external magnetic field \mathbf{H}_0 is used to tune the FMR frequency.

where $I = \int (z^2 + x^2) dz dx \simeq ad^3/12$ is again the moment of inertia of the cross-section about its center of mass and ρ is the mass density. The oscillating solution has the form $\varphi = (A_1 \sin(ky) + A_2 \cos(ky))e^{i\omega t}$, where $k = \omega/c$ is the wave number, $c = 2c_t a/d = \sqrt{C/(\rho I)}$, and $c_t = \sqrt{\mu/\rho}$ is the sound velocity of the transverse mode. The free constants A_1 and A_2 are determined by the boundary conditions.

The first condition $\varphi|_{y=L/2(-L/2)} = 0$ corresponds to perfect clamping at the boundaries. The second one, at the connection with the ferromagnetic load, can be obtained from the variational principle applied to Eq. (24), and corresponds to the torque $C\partial\varphi/\partial y|_{y=\pm L/2}$ exerted by the magnetization at the interface to the normal metal link:

$$C\frac{\partial\varphi}{\partial y}|_{y=\pm L/2} = \frac{1}{\gamma} \left(\frac{d\mathbf{M}}{dt} + \gamma\mathbf{M} \times \mathbf{H}_0 \right) |_y + L'I_F\rho_F \frac{d^2\varphi(0)}{dt^2}, \quad (30)$$

where I_F is the moment of inertia of the magnetic load (for a thin plate of mass M , we can approximate it as $L'I_F\rho_F = Md_F^2/12$, where d_F is its width, see Fig. 6), and $\partial\varphi/\partial y|_{y=\pm L/2}$ is the derivative of the torsion angle of the normal metal link at the connection with the ferromagnet. This boundary condition is equivalent to the conservation of the mechanical angular momentum written for the magnetic load. With $C\partial\varphi/\partial y|_{y=\pm L/2} = Ck\varphi \cot kL$, we obtain:

$$Ck\varphi(0) \cot(kL) - L'I_F\rho_F \frac{d^2\varphi(0)}{dt^2} = \frac{1}{\gamma} \left(\frac{d\mathbf{M}}{dt} + \gamma\mathbf{M} \times \mathbf{H}_0 \right) |_y, \quad (31)$$

where the right hand side describes the magnetically induced torques that to leading order equal the Gilbert and anisotropy torques. In the absence of the magnetic anisotropies and Gilbert damping, the two terms $d\mathbf{M}/dt$ and $\gamma\mathbf{M} \times \mathbf{H}_0$ cancel each other.

By only considering the left hand side of Eq. (31), we can find the mechanical resonance frequency as $\omega_e = \sqrt{Ck \cot(kL)/(L'I_F\rho_F)} \approx \sqrt{C/(LL'I_F\rho_F)}$, where the approximation

holds when ω_e is smaller than the resonant frequency of the normal metal link with a free end (which corresponds to the heavy-load limit). In frequency space, the left hand side of Eq. (31) can be expressed in terms of the dimensionless response function $F(\omega)$ of the mechanical subsystem to an oscillating torque of frequency ω applied to the load:

$$F(\omega) = \omega_e^2 / [(\omega^2 - \omega_e^2 + 2i\beta\omega)] \quad (32)$$

where β is a phenomenological damping constant describing dissipation in Eq. (29) and it is related to the quality factor Q of oscillator at the resonance frequency ω_e as $Q = \omega_e/(2\beta)$ (at 1 GHz $Q \sim 500$).¹⁹ In terms of $F(\omega)$, the mechanical response function reads:

$$(\varphi/T)_\omega = (1/Ck \cot(kL)) F(\omega) \approx (L/C)F(\omega), \quad (33)$$

where T is the torque externally exerted on the load.

To first order in the mechanical and magnetization oscillations, Eqs. (25) and (31) lead us to the following response function:

$$\begin{aligned} \chi_{yI}(\omega) &= (M_y/I)_\omega = \frac{\hbar\gamma}{2eV_m} \\ &\times \frac{-i\eta_1\omega + \Gamma_y\gamma [M_s + g(H_0/N_x) F(\omega)]}{\omega^2 - \omega_m^2 + 2i\alpha'\omega\omega_m + \Lambda F(\omega)} \end{aligned} \quad (34)$$

$$\stackrel{g \rightarrow 0}{\approx} \frac{\hbar \sin \theta \gamma}{2eV_m} \frac{-i\eta_1\omega + \gamma M_s \Gamma_y}{\omega^2 - \omega_m + 2i\alpha'\omega\omega_m + \Lambda F(\omega)}, \quad (35)$$

where

$$\Lambda = g [\omega^2 - H_0\omega_m/(N_x M_s)], \quad (36)$$

and

$$\begin{aligned} g &= M_s^2 V_m N_x (1/Ck \cot(kL)) \\ &\approx M_s^2 V_m N_x L/C = N_x (L/a)^2 (V_m/V_l) (M_s^2/\mu), \end{aligned} \quad (37)$$

V_m and V_l are the volumes of the magnetic load and the normal metal spring, respectively. L and a are the largest and the smallest dimensions of the normal metal links, $k = \omega_e/c$. We recover here the results from Ref. 6, implying that the spin polarized current is equivalent to an external rf field along the x -axis applied to a magnetic cantilever. Since the ratio V_m/V_l can be made much larger compared to the limit of light load considered in Ref. 6, we conclude that by making the normal metal links thinner (in setup of Ref. 6 we have to

make the cantilever thinner) we reduce the stiffness of the device, which results in a better sensitivity and stronger coupling. The reduced stiffness leads to a drop in the resonance frequency that in turn can be compensated by making the structures smaller.

The *nonlinear* response to an AC current can now be found by substituting Eq. (34) into the first parts of Eqs. (22,23). We conclude that the most conspicuous feature of the magnetovibrational coupling is the formation of a *magnetopolariton* and the splitting of the ferromagnetic resonance close to $\omega = \omega_m$, which is governed by $\sqrt{\Lambda}$. The expression for Λ , Eq. (36), suggests that the splitting can be tuned by the external magnetic field. The line width of those two resonances is defined by α' and β , and the shape is a combination of the symmetric and antisymmetric Lorentzians as in Fig. 4. Let us make estimates for a system shown in Fig. 6. The dimensions of the metallic links are here chosen as $(0.5 \times 0.05 \times 0.01) \mu\text{m}$ with a Py load of the size $(0.1 \times 0.2 \times 0.02) \mu\text{m}$, for which we can estimate a resonance frequency in the range of 0.5GHz ($\mu \sim 100\text{G Pa}$)²⁰ and a coupling parameter $g \sim 0.001$ (free-standing metallic structures of such dimensions have already been realized²¹). For intermetallic interfaces, the “effective field effect” due to η_2 is very small, thus the phase shift of the magnetization is absent ($\Gamma_y = 0$). The amplitudes, given by Eqs. (22,23), are large in the proximity of the ferromagnetic resonance (FMR). The magnetovibrational coupling splits the FMR peak by $\sqrt{g}\omega$ ($H_0 < N_x M_s$), which allows an electric detection of the mechanical motion excited by the spin transfer. Normalized voltages are plotted in Figs. 7 and 8 for purely ferromagnetic (mechanical motion is suppressed) compared to magneto-vibrational (MVR) resonances.

Finally, we write the response function for arbitrary magnetization directions in Fig. (3):

$$\chi_{y'I}(\omega) = (M_{y'}/I)_\omega = \frac{\hbar\gamma \sin \theta}{2eV_m} \quad (38)$$

$$\stackrel{g \rightarrow 0}{\approx} \frac{\hbar \sin \theta \gamma}{2eV_m} \frac{-i\eta_1\omega + \gamma M_s \Gamma_{y'}}{\omega^2 - \omega_m^2 + 2i\alpha'\omega\omega_m + \Lambda F(\omega)}, \quad (39)$$

where Λ is defined in Eq. (40). As one can see, the form of the response function does not change. Eq. (38) can be substituted into the first parts of Eqs. (22,23) in order to calculate the *nonlinear* response to an AC current. Similarly to Eq. (16), the parameter $\Gamma_{y'} \approx \eta_1 N_{x'y'} + \eta_2 N_{x'}$ governs the balance between the symmetric and antisymmetric Lorentzians

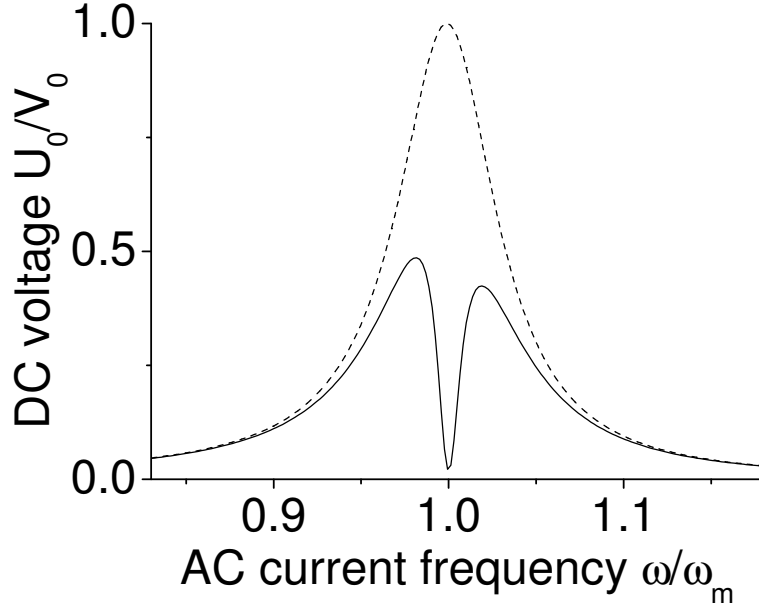


Figure 7: Dependence of the DC component of the voltage on the frequency or the AC current bias for purely FMR (dashed line) and MVR (solid line) ($\omega_m = \omega_e$, $\alpha' = 0.02$, $\beta/\omega = 0.002$, $g = 0.001$).

composing each resonance (see Fig. 4). The magnetovibrational coupling is described by Λ :

$$\text{Re } \Lambda = g [\omega^2 - (H_{z'} + \cot \theta_1 H_{y''})\omega_m / (N_{x''} M_s)] \quad (40)$$

$$\text{Im } \Lambda = g\omega\gamma [H_{z'} N_{x''y''} / N_{x''} + \cot \theta_1 (H_{x''} + H_{y''} N_{x''y''} / N_{x''})] \quad (41)$$

and

$$\begin{aligned} g &= \sin^2 \theta_1 M_s^2 V_m N_{x''} (1/Ck \cot(kL)) \\ &\approx \sin^2 \theta_1 M_s^2 V_m N_{x''} L/C = \sin^2 \theta_1 N_{x''} (L/a)^2 (V_m/V_l) (M_s^2/\mu), \end{aligned} \quad (42)$$

where V_m and V_l are the volumes of the magnetic load and the normal metal spring, respectively. L and a are the largest and the smallest dimensions of the normal metal links, $k = \omega_e/c$, θ_1 is the angle between the equilibrium direction of the magnetization \mathbf{M}_2 and the current flow, and the external field is $\mathbf{H}_0 = (H_{x''}, H_{y''}, H_{z'})$. The parameter Λ is calculated in a reference frame x'', y'', z' shown in Fig. (3). The x'' -axis is perpendicular to the current flow and the axis z' (in general, this reference frame is different from the one used in Sec. IIIA, since the x'' -axis is not necessarily along the direction of $\mathbf{m}_1 \times \mathbf{m}_2$).

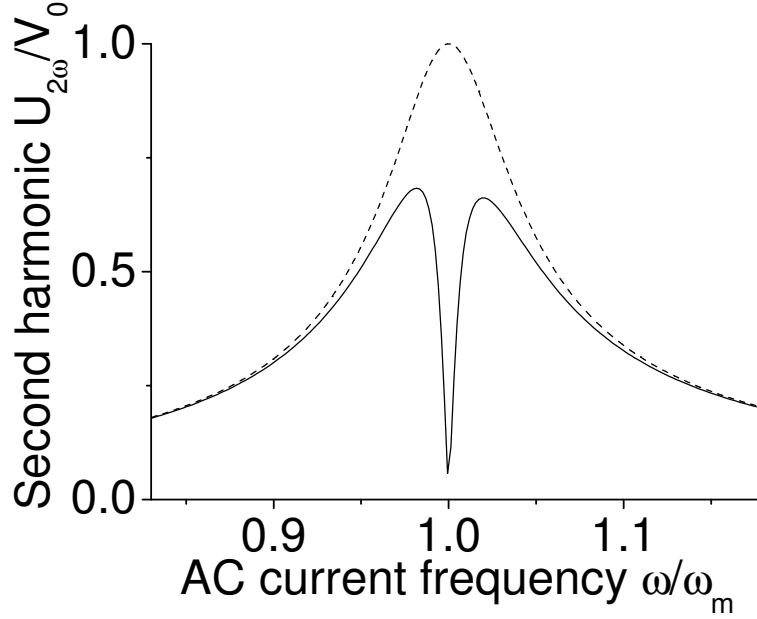


Figure 8: Dependence of the second harmonic of the voltage on the frequency of the AC current bias for purely FMR (dashed line) and MVR (solid line) ($\omega_m = \omega_e$, $\alpha' = 0.02$, $\beta/\omega = 0.002$, $g = 0.001$).

C. Mechanical torques due to absorption of transversely polarized currents

Let us now apply a DC current bias to the system in Fig. 6. According to the magnetoelastic equations discussed above, the angular momentum of the spin polarized current is completely transformed into mechanical torques when the crystal and shape anisotropies are strong enough to prevent magnetization motion relative to the lattice. The mechanical torque then equals the spin-transfer torque:

$$T_{st} = -\gamma \frac{\hbar}{2e} I \eta_1 \mathbf{m} \times (\mathbf{m}_{\text{fixed}} \times \mathbf{m}) \approx -\gamma T_0 \eta_1, \quad (43)$$

The Gilbert damping does not appear explicitly in this formula; however, it determines the time scale $1/(\alpha\gamma M_s)$ in which the system reaches quasi-equilibrium. The upper boundary for the spin-transfer-induced mechanical torque for a thin film of the size $(20 \times 200 \times 200)$ nm (without crystal anisotropy) is defined by the maximum effective magnetic field due to the form anisotropy, $H_{eff} = 4\pi\theta M_s$, where $\theta \approx \pi/20 \sim H_0/M_s$ corresponds to some small stationary deflection of the magnetization out of the plane of the film in the presence of the stabilizing external magnetic field \mathbf{H}_0 (Fig. 6). This field generates a torque of $\gamma 4\pi\theta M_s \cdot$

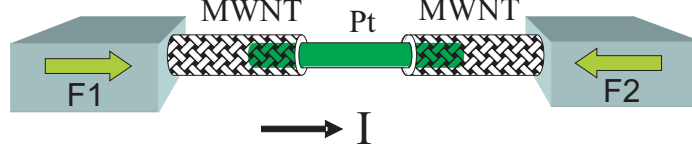


Figure 9: A spin-transfer nanomotor in which a metallic wire (rotor) with strong spin-flip scattering (such as Pt) is grown inside a MWNT that is connected to two ferromagnetic contacts.

$M_s V_m / \gamma \sim 10^{-16} \text{ N m}$, where V_m is the volume of the ferromagnet and $M_s = 10^6 \text{ A / m}$ is the saturation magnetization for Py. Such torques are well above the sensitivity of existing NEMS oscillators.²²

IV. SPIN-TRANSFER NANOMOTOR

Finally, we address the question how the torque can be transformed into a potentially useful rotary motion. It has been suggested in the literature to use carbon nanotubes as bearings for metallic nanowires.^{1,3} In Fig. 9, we propose a design of a spin-transfer nanomotor based on multi-wall carbon nanotube (MWNT) connected to two ferromagnetic electrodes (the torque doubles when the second electrode is ferromagnetic, but one ferromagnet is sufficient in principle). A metallic nanowire with strong spin-flip scattering nanowire is encapsulated by the MWNT. Pt would be a good choice ($l_{sd}^{Pt} \sim 20 \text{ nm}$ at 4.2 K²³ and $l_{sd}^{Pt} \sim 1 \text{ nm}$ at room temperature²⁴). FeCo nanowires that have already been grown inside nanotubes,²⁵ presumably have spin-flip diffusion lengths not much different from FeNi ($l_{sd}^{Py} \sim 5 \text{ nm}$),²⁶ which makes this material also very suitable. The metallic nanowire should preferably be longer than the spin-diffusion length in order to achieve a complete angular momentum transfer. After burning off the outer shells over the platinum nanowire (in addition, the MWNT may also be pulled out to open the Pt wire), we force the current to flow through the metallic wire that serves as a spin-sink and a rotor. It has recently been calculated that the conductance may rapidly oscillate due to quantum interference effects as we change the overlap between two nanotube shells,²⁷⁻²⁹ but disorder strongly enhance the intershell conductance, consistent with experiments.³⁰

The situation with not too high polarization of the MWNT connection to ferromagnet³¹ ($P \sim 0.01$) has tendency to improve with recent experiments reporting TMR = 5% ($P \sim 0.2$).³⁸⁻⁴⁰ Half-metallic contacts to nanotubes might lead to much higher values.⁴¹ Adopting

the maximum current through a single MWNT measured to date³⁴ $I = 1$ mA, we arrive at an estimate for the mechanical torque generated in the rotor $T \sim T_0 \simeq 10^{-19}$ N m where we optimistically assume $P \sim 1$. This exceeds by many orders of magnitude the torques that can be induced by circularly polarized light ($T \sim 10^{-29}$ N m).³ The advantage of a MWNT bearing is that the friction force can be very small. The bearing may still get stuck at certain preferred positions that minimize the interaction energy of the sleeve and shaft. However, each layer is likely to have a different chirality, so the potential barrier (static friction force) hindering rotation should be very small. An upper boundary for the static friction force per unit area has been measured³² to be 6.6×10^{-13} N / nm² (but the actual value is possibly much smaller). For a nanotube radius of 2 nm this corresponds to a static friction torque per unit area of less than 10^{-21} N m / nm². For the same nanotube radius, the overlap length between the rotor and the outer shells can be made at least 10 nm without the risk that the rotor gets stuck by the static friction. When the barrier to rotation is overcome, the static friction is taken over by the dynamic friction. The latter is much smaller initially, but increases proportional to the angular velocity.³³

The proposed motor could be useful in the next generation of synthetic nanometer-scale electromechanical systems. With an attached metal plate the rotor can serve as a mirror, with relevance to high-density switching devices.¹ The motor can find applications for inducing and detecting motion in microfluidics systems and biological systems.

V. CONCLUSIONS AND OUTLOOK

We find that the electric current-induced creation and detection of mechanical torques in magnetic nanostructures is possible by rectification technique suggested recently in Ref. 9 and 10. We develop a detailed theory of the magnetization dynamics in the presence of electric currents relevant for these experiments that agrees with the very recent study by Kupferschmidt *et al.*³⁵ Subsequently, we predict that an alternating current can drive magnetovibrational dynamics, which can be read out by the generated DC voltage. Finally, we come to the conclusion that electric current-induced mechanical torques can create rotary motion. We propose a novel spin-transfer driven nanomotor based on integrating metallic nanowires with carbon nanotubes.

In the study of the rectification effect, we find that the DC voltage originates from

two mechanisms: the rectification of the applied AC current and the spin-pumping by the precessing ferromagnet. The second mechanism is important only in very thin ferromagnetic layers when the Gilbert damping is strongly enhanced (in accord with Ref. 35). It should be noted that the shape of DC voltage as a function of frequency is a symmetric Lorentzian for the spin-pumping mechanism. This can be distinguished from the voltage induced in the presence of noncollinear magnetic anisotropies or the “effective” spin-transfer field, which causes asymmetric line shapes.

We generalized these results to treat magnetovibrationally coupled systems. The strongest coupling is achieved when the lowest mechanical mode is at resonance with the FMR frequency. In that case, a magnetopolariton is formed, and the Lorentzian shape of the DC voltage splits by an amount that is governed by the sensitivity of the mechanical system to external torques and by the magnetic anisotropies (without which there would be no magnetovibrational coupling). The technique based on the resonant magnetovibrational coupling can also be used to detect vibrations that are created externally. It can therefore be an alternative to the magnetomotive technique employed in fast transducers of mechanical motion.²²

We conclude that the functionalities of the spin-transfer torque, already used in applications such as magnetic memories, can be extended by taking into account the coupling with the mechanical degrees of freedom. The experimental realization is a challenge, since free-standing metallic small structures on micro and nanoscale need to be fabricated and manipulated.

Acknowledgments

We thank Yaroslav Tserkovnyak, Xuhui Wang, and Yuli Nazarov for stimulating discussions. We appreciate helpful communications with Dan Ralph and Jack Sankey. We are grateful that Piet Brouwer sent us manuscript (Ref. 35), reminding us of the importance of spin pumping. This work has been supported by the Dutch FOM Foundation, National Science Foundation Grant No. PHY99-07949, the EU Commission FP6 NMP-3 project 505587-1“SFINX”, and the Research Council of Norway Grant No. 162742/V00.

Appendix A: Effect of mixing conductance on the torque and magnetoresistance

In this Appendix, we generalize the relations derived in Ref. 14 for the torques and resistances in a general N|F1|N|F2|N multilayered structures without bulk layer spin-flip scattering to the presence of an imaginary part of the mixing conductances or “effective field”. We use magnetoelectronic circuit theory as formulated by Eqs. (11,12). Our result for the spin-transfer torque acting on the first ferromagnet (the torque on the second ferromagnet can be obtained by permutation of indexes 1 and 2, and by replacing I with $-I$) can be summarized by:

$$\mathbf{T}_{ST}^1 = \frac{I\hbar}{2e} [\eta_s \mathbf{m}_1 \times (\mathbf{m}_1 \times \mathbf{m}_2) + \eta_f (\mathbf{m}_2 \times \mathbf{m}_1)], \quad (\text{A1})$$

where we introduced the spin-transfer efficiencies:

$$\begin{aligned} \eta_s = & \left([R_{2-}(R_r + R_1) - R_{1-}R_2\alpha] \left(1 + \frac{R_{2r}}{R_r} \tilde{G}_{1i}^2\right) \right. \\ & \left. + \frac{R_{1r}}{R_r} \left[\frac{R_{2-}}{G_1} - \frac{R_{1-}}{G_2} \alpha \right] \tilde{G}_{2i}^2 + \frac{R_{1r}R_{2r}}{R_r} (R_{1-} + R_{2-}\alpha) \tilde{G}_{1i} \tilde{G}_{2i} \right) / \\ & \left((R_r + R_1)(R_r + R_2) - R_1R_2\alpha^2 + \left[\frac{(R_r + R_1)}{G_2} - \frac{R_2}{G_1} \alpha^2 \right] \frac{R_{2r}}{R_r} \tilde{G}_{1i}^2 \right. \\ & \left. + \left[\frac{(R_r + R_2)}{G_1} - \frac{R_1}{G_2} \alpha^2 \right] \frac{R_{1r}}{R_r} \tilde{G}_{2i}^2 + 2\alpha \frac{R_{1r}R_{2r}}{R_r} \left(\frac{1}{G_1} + \frac{1}{G_2} \right) \tilde{G}_{1i} \tilde{G}_{2i} \right) \\ \eta_f = & \left([R_{2-}(R_r + R_1) - R_{1-}R_2\alpha] \frac{R_{1r}}{R_r} \tilde{G}_{1i} - [R_{1-}(R_r + R_2) - R_{2-}R_1\alpha] \frac{R_{2r}}{R_r} \tilde{G}_{2i} \right. \\ & \left. + \frac{R_{1r}}{R_r} \left[\frac{R_{2-}}{G_1} - \frac{R_{1-}}{G_2} \alpha \right] \tilde{G}_{1i} \tilde{G}_{2i} - \frac{R_{2r}}{R_r} \left[\frac{R_{1-}}{G_2} - \frac{R_{2-}}{G_1} \alpha \right] \tilde{G}_{2i} \tilde{G}_{1i} \right) / \\ & \left((R_r + R_1)(R_r + R_2) - R_1R_2\alpha^2 + \left[\frac{(R_r + R_1)}{G_2} - \frac{R_2}{G_1} \alpha^2 \right] \frac{R_{2r}}{R_r} \tilde{G}_{1i}^2 \right. \\ & \left. + \left[\frac{(R_r + R_2)}{G_1} - \frac{R_1}{G_2} \alpha^2 \right] \frac{R_{1r}}{R_r} \tilde{G}_{2i}^2 + 2\alpha \frac{R_{1r}R_{2r}}{R_r} \left(\frac{1}{G_1} + \frac{1}{G_2} \right) \tilde{G}_{1i} \tilde{G}_{2i} \right) \end{aligned}$$

with $\alpha = \cos \theta$, $4R_{1(2)} = 1/G_{1(2)\uparrow} + 1/G_{1(2)\downarrow} - 2/G_{1(2)r}$, $4R_{1(2)-} = 1/G_{1(2)\uparrow} - 1/G_{1(2)\downarrow}$, $4/G_{1(2)} = 1/G_{1(2)\uparrow} + 1/G_{1(2)\downarrow}$, $2R_{1(2)r} = 1/G_{1(2)r}$, $2R_r = 1/G_{1r} + 1/G_{2r}$ and $\tilde{G}_{1(2)i} = G_{1(2)i}/G_{1(2)r}$, where $G_{1(2)\uparrow}$ and $G_{1(2)\downarrow}$ are conductances of the left (right) ferromagnet including the left (right) normal layer (when necessary, the middle layer conductance can also be included in these conductances), $G_{1(2)\uparrow\downarrow} = G_{1(2)r} + iG_{1(2)i}$ is the mixing conductance of the left (right) ferromagnet.

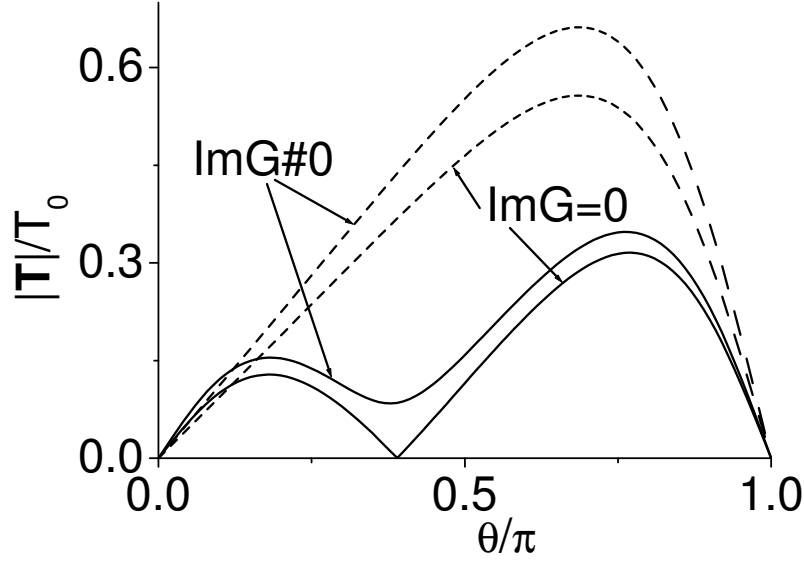


Figure 10: Enhancement of the torque by a nonzero imaginary part of the spin-mixing conductance; dashed line for symmetric ($P = R_- G = 0.7$, $G/G_r = 0.6$, $\tilde{G}_i = 0.6$) and solid line for asymmetric junctions ($P_1 = R_{1-} G_1 = 0.6$, $G_1/G_{1r} = G_1/G_{2r} = 0.6$, $\tilde{G}_{1i} = -\tilde{G}_{2i} = 0.4$, $G_1 = 2G_2$, $P_2 = R_{2-} G_2 = 0.13$).

The angular magnetoresistance reads:

$$\begin{aligned}
 R(\theta) = & R_r + R_1 + R_2 - \left([R_{1-}^2 + R_{2-}^2 + 2R_{1-}R_{2-}\alpha] \left(1 + \frac{R_{2r}^2}{R_r^2} \tilde{G}_{1i}^2 + \frac{R_{1r}^2}{R_r^2} \tilde{G}_{2i}^2 \right) \right. \\
 & + \frac{(1-\alpha^2)}{R_r^2} \left([R_{1-}^2 R_2 + R_{2-}^2 R_1] [R_r + R_{2r} \tilde{G}_{1i}^2 + R_{1r} \tilde{G}_{2i}^2] + R_{1-}^2 R_{1r} R_{2r} \tilde{G}_{2i}^2 + R_{2-}^2 R_{1r} R_{2r} \tilde{G}_{1i}^2 \right) \\
 & \left. + 2(R_{1-} + R_{2-}\alpha)(R_{2-} + R_{1-}\alpha) \frac{R_{1r} R_{2r}}{R_r^2} \tilde{G}_{1i} \tilde{G}_{2i} \right) / \\
 & \left(\left(1 + \frac{R_1}{R_r} \right) (R_r + R_2) - \frac{R_1}{R_r} R_2 \alpha^2 + \left[\frac{(R_r + R_1)}{G_2} - \frac{R_2}{G_1} \alpha^2 \right] \frac{R_{2r}}{R_r^2} \tilde{G}_{1i}^2 \right. \\
 & \left. + \left[\frac{(R_r + R_2)}{G_1} - \frac{R_1}{G_2} \alpha^2 \right] \frac{R_{1r}}{R_r^2} \tilde{G}_{2i}^2 + 2\alpha \frac{R_{1r} R_{2r}}{R_r^2} \left(\frac{1}{G_1} + \frac{1}{G_2} \right) \tilde{G}_{1i} \tilde{G}_{2i} \right)
 \end{aligned} \tag{A2}$$

When the imaginary part of the mixing conductance is small, the absolute value of the torque Eq. (A1) and the magnetoresistance Eq. (A2) contain only second order corrections in \tilde{G}_{1i} and \tilde{G}_{2i} . In general, we conclude that the torque is enhanced when the imaginary part is not zero, as it is shown in Fig. 10. This enhancement makes it impossible to have noncollinear points of zero torque reported earlier^{14,42} (see Fig. 10) which can influence the

stable precessional states.

Appendix B: Spin pumping and DC voltage in asymmetric N|F|N structures

We consider here an asymmetric N1|F|N2 layered structure connected to two reservoirs and excited by rf magnetic fields. We are interested in the DC voltage that builds up under the condition of zero charge current. The system can be described by the generalized LLG equation and magnetoelectronic circuit theory:

$$\frac{d\mathbf{M}}{dt} = -\gamma\mathbf{M} \times \mathbf{H}_{\text{eff}} + \frac{\alpha}{M_s}\mathbf{M} \times \left(\frac{d\mathbf{M}}{dt}\right) - \frac{\gamma\hbar}{2eV_m}\mathbf{m} \times [(\mathbf{I}_{s1} + \mathbf{I}_{s2}) \times \mathbf{m}] \quad (\text{B1})$$

$$I_{1(2)} = (G_{\uparrow} + G_{\downarrow})(\mu_0^{2(1)} - \mu_0^{1(2)}) + (G_{\uparrow} - G_{\downarrow})(\boldsymbol{\mu}_s^{2(1)} - \boldsymbol{\mu}_s^{1(2)}) \cdot \mathbf{m} \quad (\text{B2})$$

$$\begin{aligned} \mathbf{I}_{s1(2)} = \mathbf{m} \Big[& (G_{\uparrow} - G_{\downarrow})(\mu_0^{2(1)} - \mu_0^{1(2)}) + (G_{\uparrow} + G_{\downarrow})(\boldsymbol{\mu}_s^{2(1)} - \boldsymbol{\mu}_s^{1(2)}) \Big] \\ & - (2\mathbf{m} \times \boldsymbol{\mu}_s^{1(2)} - \hbar\dot{\mathbf{m}}) \times \mathbf{m}G_r - (2\mathbf{m} \times \boldsymbol{\mu}_s^{1(2)} - \hbar\dot{\mathbf{m}}) G_i, \end{aligned} \quad (\text{B3})$$

where G_{\uparrow} and G_{\downarrow} describe the spin-dependent conductance limited by interface and bulk scattering of the ferromagnet, $G_{\uparrow\downarrow} = G_r + iG_i$ is the interface mixing conductance of the ferromagnet, the vector $\mathbf{m} = \mathbf{M}/M_s$ is the direction of the magnetization, μ_0 and $\boldsymbol{\mu}_s$ are the chemical potential and spin-accumulation in the normal metals, respectively.

For metallic interfaces, G_i usually amounts to only a few percent of G_r . We calculate here the linear response to the external rf magnetic field when G_i is disregarded:

$$\chi_{xx}(\omega) = (M_x/h_x)_{\omega} = \frac{(\gamma M_s)^2(N_y + N_{xy}\alpha)}{\omega^2(1 + \alpha_{se}^2) - \omega_m^2(1 + \alpha^2) + 2i\alpha'\omega\omega_m}. \quad (\text{B4})$$

$$\chi_{yx}(\omega) = (M_y/h_x)_{\omega} = \frac{\gamma M_s [\gamma M_s(N_{xy} + N_x\alpha) - i\omega]}{\omega^2(1 + \alpha_{se}^2) - \omega_m^2(1 + \alpha^2) + 2i\alpha'\omega\omega_m}. \quad (\text{B5})$$

where α is the bulk Gilbert damping, $\alpha_{se} = \gamma\hbar^2(G_1 + G_2)/(2eM_sV)$ is the extra damping due to spin-emission, $1/G_1 = 1/g_1 + 1/2G_r$, $1/G_2 = 1/g_2 + 1/2G_r$ with g_1 and g_2 being conductances of the R1|N1 and N2|R2 interfaces, respectively, $\alpha' = (\alpha + \alpha_{se})(N_x + N_y)/(2\sqrt{N_xN_y - N_{xy}^2})$ (note that, when important, bulk scattering can be easily included into the conductances g_1 , g_2 and G_r).^{14,43}

By solving Eqs. (B1-B3) to the second order in a small rf magnetic field the generated DC voltage can be expressed via the susceptibilities Eqs. (B5) and (B4) as:

$$eV = 2\hbar\omega PG_r \left(\frac{1}{g_1} - \frac{1}{g_2} \right) \text{Im}(\chi_{xx}\chi_{yx}^*) h_x^2/M_s^2, \quad (\text{B6})$$

where we introduced the effective polarization of the device $P = (1/G_{\uparrow} - 1/G_{\downarrow})/(1/G_{\uparrow} + 1/G_{\downarrow} + 4/g_1 + 4/g_2)$. The asymmetry of the interfaces R1|N1 and N2|R2 is seen to be crucial for the generation of a DC voltage in this geometry. Note that the dependence of the DC voltage on the frequency has a Lorentzian line shape as follows from Eqs. (B4-B6). When $P > 0$, the positive sign of the voltage corresponds to the voltage applied to the junction with higher conductance $g_{1(2)}$.

The first order correction in the mixing conductance G_i leads to a slight change of the height of the Lorentzian and to a shift of the resonance frequency:

$$\omega^2 = \omega_m^2 \left(1 - \frac{\gamma \hbar^2 (G_1^2 + G_2^2)}{4eM_s V_m} \frac{G_i}{G_r^2} \right) \quad (\text{B7})$$

Note that the magnetovibrational coupling does not change the form Eq. (B6), when the proper susceptibilities Eqs. (34) are substituted. The magnetovibrational coupling can thus be observed as a splitting of the Lorentzian peak due to spin pumping in an asymmetric N1|F|N2 structure. Generation of a DC voltage by magnetization precession of a single ferromagnetic layer has been suggested in Ref. 37. However, those authors concentrate on the generation of a DC voltage due to spin-flip scattering in the ferromagnet.

Appendix C: Spin pumping and rectification of AC currents in F|N|F|N structures

It follows from the previous appendix on N1|F|N2 structures that a spin-coherent F1|N|F2|N structures in which the normal metals are identical and an extra ferromagnetic layer F1 (with fixed magnetization) causes the asymmetry, should generate a DC voltage as well. In such a structure, AC currents instead of the rf magnetic field can generate spin transfer torques when the magnetizations are non-collinear. Since the analytical expressions for arbitrary angles between the magnetizations are complex, we concentrate here, without loss of generality, on a 90 degree configuration.

We assume a constant AC current bias on the system, thus forcing the extra charge current due to spin pumping to vanish. Following the derivation in Appendix B, and disregarding the imaginary parts of mixing conductances for both interfaces, we arrive at the following expressions for the linear response functions:

$$\chi_{xI}(\omega) = (M_y/I)_{\omega} = \frac{\hbar\gamma}{2eV_m} \frac{\eta_1 [\gamma M_s (N_y + N_{xy}\alpha) - i\omega\alpha_x^{se}]}{\omega^2(1 + \alpha_x^{se}\alpha_y^{se}) - \omega_m^2(1 + \alpha^2) + i\omega\Delta}, \quad (\text{C1})$$

$$\chi_{yI}(\omega) = (M_x/I)_\omega = \frac{\hbar\gamma}{2eV_m} \frac{\eta_1 [\gamma M_s (N_{xy} + N_x \alpha) - i\omega]}{\omega^2(1 + \alpha_x^{se} \alpha_y^{se}) - \omega_m^2(1 + \alpha^2) + i\omega\Delta}, \quad (C2)$$

where the anisotropic Gilbert dampings due to spin emission are $\alpha_x^{se} = \gamma\hbar^2(G_1 + G_2)/(2eM_sV_m)$, $\alpha_y^{se} = \gamma\hbar^2(G_{\uparrow\downarrow} + G_2)/(2eM_sV_m)$, $\Delta = \gamma M_s(N_x(\alpha + \alpha_x^{se}) + N_y(\alpha + \alpha_y^{se}) + \alpha(\alpha_y^{se} - \alpha_x^{se})N_{xy})$, $1/G_1 = (1/g_{1\uparrow} + 1/g_{1\downarrow})/4 + 1/2G_r$, $1/G_2 = 1/g_2 + 1/2G_r$, $1/G_{\uparrow\downarrow} = 1/2G_r + 1/2g_{1r}$ with $g_{1\uparrow\downarrow} = g_{1r} + ig_{1i}$ (however g_{1i} is neglected) and $g_{1\uparrow(\downarrow)}$ being the mixing and normal conductances of the R1|F interface, respectively.

The second order analysis provides us with an expression for the DC voltage. After combining it with Eq. (22), we arrive at the full expression for the DC voltage in terms of the susceptibilities Eqs. (C1,C2), consisting of separate contributions due to rectification and spin pumping:

$$U_0 = \frac{I_0^2}{2M_s} \frac{\partial R(\nu)}{\partial \nu} \text{Re } \chi_{yI} + \frac{2\hbar\omega}{e} P G_r \left(\frac{1}{\tilde{g}_1} - \frac{1}{g_2} \right) \text{Im}(\chi_{xI} \chi_{yI}) I_0^2 / M_s^2, \quad (C3)$$

where an effective conductance is $1/\tilde{g}_1 = (3/2g_{1r} + (1/4g_{1\uparrow} + 1/4g_{1\downarrow})R_{\uparrow\downarrow}/R_1)/4$ and an effective polarization of the device is $P = (1/4G_{\uparrow} - 1/4G_{\downarrow})/(1/4G_{\uparrow} + 1/4G_{\downarrow} + 1/2g_{1r} + 1/g_2)$. The dependence of the first term in Eq. (C3) on the frequency is in general a combination of the Lorentzian with an antisymmetric Lorentzian, as it is discussed in the Section IIIA. The second term becomes important when $\alpha^{se} \gtrsim \alpha$ and $\frac{1/\tilde{g}_1 - 1/g_2}{1/g_{1\uparrow} - 1/g_{1\downarrow}} \gtrsim 1$. When the damping due to spin emission is small or the asymmetry of the tri-layer weak, the second term in Eq. (C3) can be disregarded. Its dependence on the frequency has a Lorentzian shape, see Eqs. (C1,C2). In general, the signs of the first and second term in Eq. (C3) can be opposite, thus possible suppressing the symmetric-Lorentzian part of DC voltage.

The first order corrections in a small mixing conductances, G_i and g_{1i} lead to a change of the height of the symmetric and antisymmetric parts of Lorentzian and also to a shift of the resonance frequency, as it arises from the expressions for the susceptibilities:

$$\chi_{xI}(\omega) = (M_y/I)_\omega = \frac{\hbar\gamma}{2eV_m} \frac{i\omega(\eta_2 - \eta_1\alpha_x^{se}) + \gamma M_s \Gamma_x}{\omega^2(1 + \alpha_x^{se} \alpha_y^{se} + 2\kappa) - \omega_m^2(1 + \alpha^2) + i\omega\Delta}, \quad (C4)$$

$$\chi_{yI}(\omega) = (M_x/I)_\omega = \frac{\hbar\gamma}{2eV_m} \frac{-i\omega(\eta_1 + \eta_1\kappa - \eta_2\alpha_y^{se}) + \gamma M_s \Gamma_y}{\omega^2(1 + \alpha_x^{se} \alpha_y^{se} + 2\kappa) - \omega_m^2(1 + \alpha^2) + i\omega\Delta}, \quad (C5)$$

where $\kappa = \gamma \frac{\hbar^2}{4eM_sV_m} \left(\frac{1}{R_{\uparrow\downarrow}R_1} + \frac{1}{R_2^2} \right) \frac{G_i}{G_r^2}$, $\Gamma_x = \eta_1(N_y + N_{xy}\alpha) + \eta_2(N_{xy} - N_y\alpha)$ and $\Gamma_y = \eta_1(N_{xy} + N_x\alpha) + \eta_2(N_x - N_{xy}\alpha)$.

Finally, we present our results in the presence of the magnetovibrational coupling (*e.g.* see Fig. 6) keeping only the dominant terms in small Gilbert damping:

$$\begin{aligned}\chi_{xI}(\omega) &= \frac{\hbar \sin \theta \gamma}{2eV_m} \\ &\times \frac{i\omega(\eta_2 - \eta_1 \alpha_x^{se}) + g(1 - N_{xy}/N_x)F(\omega) + \gamma M_s \Gamma_x}{\omega^2(1 + \kappa) - \omega_m^2 + i\omega\Delta + \Lambda F(\omega)} \\ &\stackrel{g \rightarrow 0}{\approx} \frac{\hbar \sin \theta \gamma}{2eV_m} \frac{\eta_2 i\omega + \gamma M_s \Gamma_x}{\omega^2 - \omega_m + i\omega\Delta + \Lambda F(\omega)},\end{aligned}\tag{C6}$$

$$\begin{aligned}\chi_{yI}(\omega) &= \frac{\hbar \sin \theta \gamma}{2eV_m} \\ &\times \frac{-i\omega(\eta_1 + \eta_1 \kappa + \eta_2 \alpha_y^{se}) + \gamma M_s \Gamma_y [1 + g(H_z/M_s N_x^1) F(\omega)]}{\omega^2(1 + 2\kappa) - \omega_m^2 + i\omega\Delta + \Lambda F(\omega)} \\ &\stackrel{g \rightarrow 0}{\approx} \frac{\hbar \sin \theta \gamma}{2eV_m} \frac{-\eta_1 i\omega + \gamma M_s \Gamma_y}{\omega^2 - \omega_m + i\omega\Delta + \Lambda F(\omega)}.\end{aligned}\tag{C7}$$

These susceptibilities can be used in Eq. (C3) in order to calculate the generated DC voltage. In the regime of resonant magnetovibrational coupling, the second (spin emission) term in Eq. (C3) is comparable with the first one only when $\alpha^{se} \sim \beta/\omega_m$. The second term corresponds to two symmetric Lorentzian peaks split by $\text{Re } \Lambda$.

Spin pumping therefore can play an important role when the enhanced interface damping is comparable to the bulk Gilbert damping and, in the regime of magnetovibrational coupling, the mechanical damping.

-
- ¹ A. M. Fennimore, T. D. Yuzvinsky, W.-Q. Han, M. S. Fuhrer, J. Cumings, and A. Zettl, *Nature* **424**, 408 (2003).
 - ² Z. Xu and Q. Zheng (2006), cond-mat/0606302.
 - ³ P. Král and H. R. Sadeghpour, *Phys. Rev. B* **65**, 161401 (2002).
 - ⁴ P. Mohanty, G. Zolfagharkhani, S. Kettemann, and P. Fulde, *Phys. Rev. B* **70**, 195301 (2004).
 - ⁵ A. G. Mal'shukov, C. S. Tang, C. S. Chu, and K. A. Chao, *Phys. Rev. Lett.* **95**, 107203 (2005)
 - ⁶ A. A. Kovalev, G. E. W. Bauer, and A. Brataas, *Jpn. J. Appl. Phys.* **45**, 3878 (2006).
 - ⁷ M. D. Stiles and A. Zangwill, *J. Appl. Phys.* **91**, 6812 (2002).
 - ⁸ A. A. Kovalev, G.E.W. Bauer, and A. Brataas, *Appl. Phys. Lett.* **83**, 1584 (2003).
 - ⁹ A. A. Tulapurkar, Y. Suzuki, A. Fukushima, H. Kubota, H. Maehara, K. Tsunekawa, D. D. Djayaprawira, N. Watanabe, and S. Yuasa, *Nature* **438**, 339 (2005).

- ¹⁰ J. C. Sankey, P. M. Braganca, A. G. F. Garcia, I. N. Krivorotov, R. A. Buhrman, and D. C. Ralph, Phys. Rev. Lett. **96**, 227601 (2006).
- ¹¹ Y. Tserkovnyak, A. Brataas, and G. E. W. Bauer, Phys. Rev. Lett. **88**, 117601 (2002)
- ¹² L. D. Landau and E. M. Lifshitz, *Theory of Elasticity* (Pergamon, Oxford, 1959), 2nd ed.
- ¹³ A. Brataas, Y. V. Nazarov, and G. E. W. Bauer, Eur. Phys. J. B **22**, 99 (2001); A. Brataas, G. E. W. Bauer, and P.J. Kelly, Phys. Rep. **427**, 157 (2006).
- ¹⁴ A. A. Kovalev, A. Brataas, and G. E. W. Bauer, Phys. Rev. B **66**, 224424 (2002).
- ¹⁵ X. Wang, G. E. W. Bauer, and A. Hoffmann, Phys. Rev. B **73**, 054436 (2006).
- ¹⁶ X. Wang, G. E. W. Bauer, and T. Ono, Jpn. J. Appl. Phys. **45**, 3863 (2006).
- ¹⁷ J. C. Slonczewski, J. Magn. Magn. Mater. **159**, L1 (1996).
- ¹⁸ J. C. Slonczewski, Phys. Rev. B **71**, 024411 (2005).
- ¹⁹ X. Ming, H. Huang, C. A. Zorman, M. Mehregany and M. L. Roukes, Nature **421**, 496 (2003).
- ²⁰ M. G. Simmons and H. Wang, *Single crystal elastic constants and calculated aggregate properties* (MIT Press, 1975).
- ²¹ G. S. Paraoanu, and A. M. Halvari, Appl. Phys. Lett. **86**, 093101 (2005).
- ²² X. M. H. Huang, X. L. Feng, C. A. Zorman, M. Mehregany, and M. L. Roukes, New J. Phys. **7**, 247 (2005).
- ²³ S. K. Olson, R. Loloee, N. Theodoropoulou, W. P. Pratt, Jr., J. Bassa, P. X. Xu, and Ke Xia, Appl. Phys. Lett. **87**, 252508 (2005).
- ²⁴ S. Mizukami, Y. Ando, and T. Miyazaki, Phys. Rev. B **66**, 104413 (2002).
- ²⁵ A. L. Elías, J. A. Rodríguez-Manzo, M. R. McCartney, D. Golberg, A. Zamudio, S. E. Baltazar, F. López-Urías, E. Munõz-Sandoval, L. Gu, C. C. Tang, et al., Nano Lett. **5**, 467 (2005).
- ²⁶ S. Urazhdin, R. Loloee, and W. P. Pratt, Jr., Phys. Rev. B **71**, 100401 (2005).
- ²⁷ D.-H. Kim and K. J. Chang, Phys. Rev. B **66**, 155402 (2002).
- ²⁸ R. Tamura, Y. Sawai, and J. Haruyama, Phys. Rev. B **72**, 045413 (2005).
- ²⁹ M. A. Tunney and N.R. Cooper (2006), cond-mat/0606410.
- ³⁰ J. Cumings and A. Zettl, Phys. Rev. Lett. **93**, 086801 (2004).
- ³¹ K. Tsukagoshi, B. W. Alphenaar, and H. Ago, Nature **401**, 572 (1999).
- ³² J. Cumings and A. Zettl, Science **289**, 602 (2000).
- ³³ J. Servantie and P. Gaspard (2006), cond-mat/0606234.
- ³⁴ S. Dohn, K. Mølhave, and P. Bøggil, Sensor Lett. **3**, 300 (2005).

- ³⁵ J. N. Kupferschmidt, S. Adam, and P. W. Brouwer, cond-mat/0607145.
- ³⁶ G. E. W. Bauer, A. Brataas, Y. Tserkovnyak, and B. J. van Wees, Appl. Phys. Lett. **82**, 3928 (2003).
- ³⁷ X. Wang, G. E. W. Bauer, B. J. van Wees, A. Brataas, and Y. Tserkovnyak, cond-mat/0608022.
- ³⁸ S. Sahoo, T. Kontos, J. Furer, C. Hoffmann, M. Gräber, A. Cottet, and C. Schönenberger, Nat. Phys. **1**, 99 (2005).
- ³⁹ N. Tombros, S. J. van der Molen, and B. J. van Wees, Phys. Rev. B **73**, 233403 (2006).
- ⁴⁰ H. T. Man, I. J. W. Wever, and A. F. Morpurgo, Phys. Rev. B **73**, 241401 (2006).
- ⁴¹ L. E. Hueso, G. Burnell, J. L. Prieto, L. Granja, C. Bell, D. J. Kang, M. Chhowalla, S. N. Cha, J. E. Jang, G. A. J. Amaratunga, and N. D. Mathur, Appl. Phys. Lett. **88**, 083120 (2006).
- ⁴² J. Manschot, A. Brataas, and G. E. W. Bauer, Phys. Rev. B **69**, 092407 (2004).
- ⁴³ A. A. Kovalev, G. E. W. Bauer, and A. Brataas, Phys. Rev. B **73**, 054407 (2006).